An improved algorithm for VIIRS Day/Night Band (DNB) high gain stage (HGS) dark offset determination

Yalong Gu[a], Sirish Uprety[b], Slawomir Blonski[a], Bin Zhang[a], and Changyong Cao[c]
[a]Earth Resources Technology, Inc., Laurel, MD USA 20707
[b]Department.of Astronomy, University of Maryland, College Park, MD USA 20740
[c]Center for Satellite Application and Research, NESDIS/NOAA, College Park, MD UDA 20740

ABSTRACT

With comprehensive analysis of the VIIRS DNB on-board calibrator blackbody (OBCBB) data and Earth View (EV) data, it is shown that the DNB OBCBB data can only track the dark current component of the DNB HGS EV dark offset. The DNB observation of deep space during the spacecraft pitch maneuver was also contaminated by star lights. With these acquired knowledge, we propose an improved algorithm for determining the DNB HGS dark offset that is both free from light contamination and capable of tracking drifts continously. The new algorithm is expected to improve the DNB radiometric performance at low radiance level.

Keywords: Radiometric calibration, dark offset, dark current

1. INTRODUCTION

The Day/Night Band (DNB) is a panchromatic visible and near-infrared band of the Visible Infrared Imaging Radiometer Suite (VIIRS) on-board the Suomi National Polar-orbiting Partnership (S-NPP) satellite. It is effectively an integration of three separate bands which have the same spectral range and measure incident radiances independently. They are Low-Gain Stage (LGS) for daytime scenes, Mid-Gain Stage (MGS) for twilight scenes and High-Gain Stage (HGS) for nighttime scenes. As a unity, the DNB is able to cover a wide range of radiance measurement from 3×10^{-9} $W \cdot cm^{-2} \cdot sr^{-1}$ to 2×10^{-2} $W \cdot cm^{-2} \cdot sr^{-1}$ [1][2]. One of the most intriguing features of the DNB is its extreme sensitivity to low light. It begins a new era of Earth remote sensing at nighttime. An example of its application is monitoring of power outages after natural disasters [3].

The DNB's excellent low light detection ability benefits from the special design of its HGS. The HGS consists of two identical CCD arrays whose size is 672 (track) × 250 (scan), namely High-Gain Stage A (HGA) and High-Gain Stage B (HGB) which in practice are combined to a single output known as HGS for Earth observations. The 250 along-scan detectors allow repeated measurement of the same target, effectively increasing the exposure time. It is such so-called time delay integration (TDI) that enhances the sensitivity to low light signals [4]. However, the cost of long exposure time is susceptibility of the HGS to radiation damage from energetic particles in the space environment. A deleterious effect of such damage is continuously increased dark offset, which is a key parameter that needs to be determined for the DNB HGS radiometric calibration [5].

Dark offset of an imaging radiometer is usually estimated by its measurement of dark target. The original algorithm for the DNB dark offset calibration uses the Pacific Ocean as a dark target. In particular, the measurement is performed during nighttime of new moon when the moon light contamination is excluded. However, it was discovered that such target is not sufficiently dark due to airglow in the Earth atmosphere. In addition, such measurement is performed every lunar month through a special process known as the VIIRS recommended operating procedure (VROP). Offline processing is required for update of the DNB dark offsets of all three gain stages. To overcome the aforementioned drawbacks, an alternative method has been developed, which first determines the baseline HGS dark offset by the DNB observation of deep space collected during the spacecraft pitch maneuver early in the mission and then tracks its on-orbit drift due to radiation damage from energetic particles in space environment by the onboard calibrator blackbody (OBCBB) data collected when the spacecraft is in Earth eclipse and the Moon is less than quarter [6]. Because the OBCBB data are recorded in real time, the alternative method can be run automatically to update the DNB HGS dark offset. The derived HGS dark offset is also free from airglow as there is no atmosphere in deep space.

Earth Observing Systems XXIII, edited by James J. Butler, Xiaoxiong (Jack) Xiong, Xingfa Gu, Proc. of SPIE Vol. 10764, 107641J · © 2018 SPIE · CCC code: 0277-786X/18/$18 · doi: 10.1117/12.2322923

The alternative method is based on the assumption that the DNB OBCBB data can monitor the EV HGS dark offset drift. However, without thorough analysis of the relationship between the DNB OBCBB and EV data, such assumption is questionable considering the electronic timing difference between these two views. In addition, it is unclear if the deep space is dark enough for HGS given star lights in space environment and the extreme sensitivity of HGS to low lights. This paper is devoted to address the above concerns. Through comprehensive analysis, we have shown that the DNB OBCBB data can only track the dark current component of the DNB HGS EV dark offset, instead of the total dark offset. The DNB observation of deep space during the spacecraft pitch maneuver was also contaminated by star lights in space environment. With these acquired knowledge, in this paper we propose an improved algorithm for determining the DNB HGS dark offset. By combined use of the DNB OBCBB data and the DNB VROP data, the generated DNB HGS dark offset is both free from light contamination and capable of tracking continuous drift. The improved algorithm could potentially improve the DNB radiometric performance at low radiance level.

2. OVERVIEW OF VIIRS DNB DAKR OFFSET CALIBRATION

On orbit, the DNB, as well as other VIIRS bands, collects data via a rotating telescope assembly and a two-side half angle mirror (HAM) which scans four windows of view, OBCBB, solar diffuser (SD), space view (SV) and EV successively [4]. The first three are known as the onboard calibrators designed for the VIIRS on-orbit calibration [7]. As implied by the name, the EV is used for Earth observation. The entire swath width of an EV scan is about 3000 kilometers. In order to eliminate the bow-tie effect and keep a constant ground resolution across scan, the whole EV is divided into 32 aggregation zones on each side of the nadir where a different number of detectors is grouped according to the specific aggregation mode [8]. After aggregation, the size of a single-scan DNB EV data is 16 × 4064 (track × scan). The 16 along-track pixels are created by on-board aggregation of 672 along-track detectors. Unless otherwise specified, the actual detectors are named as "subpixels", while the term "detector" used in the rest of the paper is referred to as 16 virtual along-track detectors, both following the VIIRS nomenclature [4].

Because of the radiation induced dark offset drift, the DNB HGS dark offset as well as MGS and LGS dark offset are originally evaluated by the measurement of the Pacific Ocean during nighttime of every new moon (VROP). As these VROP data are collected over the EV window, the size of these dark offsets is 16 detectors × 4064 samples × 2 HAM side. They can be used for DNB EV calibration directly, thereafter referred to as the EV dark offsets. It was soon discovered that the dark Earth scenes collected during VROPs include airglow that can be detected by the DNB HGS, resulting in biased HGS dark offset for its EV calibration. The OBCBB operates with nominal temperature 292.5 K. According to the Plank's law, its emitted radiance in the DNB spectral range is undetectable even by the HGS. Therefore it is a suitable dark object for the DNB. Processing the DNB OBCBB data collected when the spacecraft is in Earth eclipse yields another set of the DNB dark offset, known as the BB dark offset. Because the OBCBB window is much narrower than the EV window, the DNB gain stages only collect 16 samples of a specific aggregation mode over a scan. The size of the BB dark offset of each gain stage is 32 aggregation modes × 16 detectors × 2 HAM side.

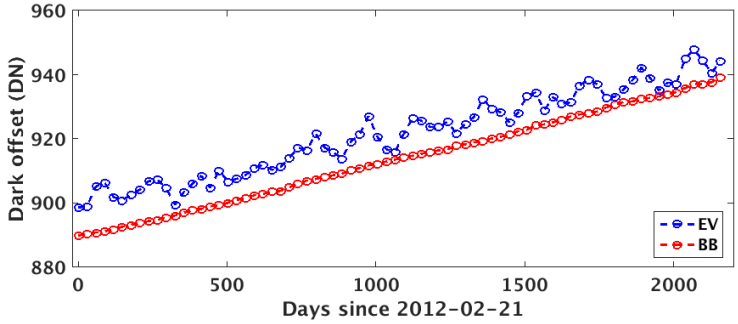

Figure 1. Time series of the measured EV and BB HGS dark offset for detector 1, aggregation mode 1 and HAM A.

Due to different size and electronic timing, the BB dark offset cannot be used for DNB EV calibration directly. As an alternative, it is used to track the on-orbit change of the DNB HGS EV dark offset. Because the HGS OBCBB data is contaminated by moon light, only the BB HGS dark offsets determined around new moon are used for tracking purpose. On the other hand, a baseline EV HGS dark offset free of airglow was determined by the DNB EV scenes of deep space

collected during the spacecraft pitch maneuver early in the mission. Upon adding the on-orbit drift estimated by the BB HGS dark offset to the baseline EV HGS dark offset, the estimated EV HGS dark offset at a given time is obtained.

The pitch maneuver based algorithm relies on an assumption that the BB HGS dark offset can track the EV HGS dark offset. Figure 1 shows the time series of these two dark offsets from February 2012 to January 2018, calculated for each new moon. Although the EV HGS dark offset evaluated by the monthly VROP data experiences short-term fluctuations, which are due to airglow, its long-term drift is similar to the BB HGS dark offset drift. The dark offsets shown in Figure 1 belong to aggregation mode 1. Their correlation coefficient is 0.97. Such high correlation coefficient suggests that the aggregation mode 1 of the EV HGS dark offset may be tracked by the BB HGS dark offset of the same aggregation mode. We repeated such calculation of correlation for all 32 aggregation modes, 16 detectors and 2 HAM sides. The results of all aggregation modes/detectors for HAM A are shown in Figure 2. It can be seen that the correlation coefficient decreases as the aggregation mode increase. This is understandable. Large aggregation mode corresponds to large scan angle which means long path between the Earth surface and the on-orbit instrument. Since the detected airglow is the airglow integrated over the whole path, the EV HGS dark offsets of large aggregation modes evaluated by the VROP data include more airglow which is not correlated to the corresponding BB HGS dark offsets. As a result, the correlation coefficient becomes smaller. However, abnormal correlation coefficients are observed for all detectors of aggregation modes 29 to 32. They are as high as 0.95 and as low as 0.65. Such large variation can't be explained by the detected airglow. It suggests that relationship between the EV and BB HGS dark offsets must be thoroughly investigated before using the BB HGS dark offset to track the EV HGS dark offset drift.

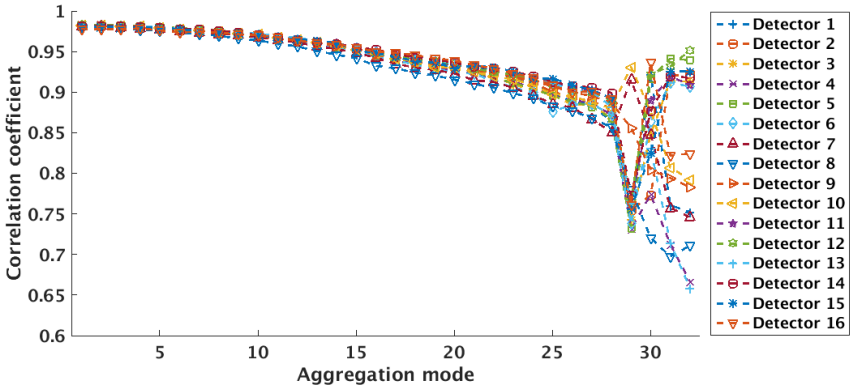

Figure 2. Correlation coefficient between the EV and BB HGS dark offset for all detectors and aggregation modes. The HAM side is HAM A.

3. RELATIONSHIP BETWEEN THE EV AND BB HGS DARK OFFSET

To begin with, it is worthy to introduce the definition of CCD dark offset. It is evaluated through measurement of dark object, namely dark images. A CCD dark image usually contains three main components, thermal dark charge, offset level and fixed pattern noise [9]. Thermal dark charge, also known as dark current, is referred to as free electrons generated in CCD sensor by thermal energy. Its magnitude is proportional to integration time and strongly depends on temperature. Offset level and fixed pattern noise are produced by CCD electronics and therefore independent of integration time. Dark offset can be mathematically expressed by the following equation

$$\text{dark\_offset} = N_{DC} + N_{bias} + N_{contam}, \quad (1)$$

where N_{DC} stands for dark current. Because both offset level and fixed pattern noise are generated by CCD electronics, they are combined into a single term N_{bias}, named as the electronic bias in this paper. Here we added a light contamination term N_{contam} which accounts for possible light contamination included in dark images such as airglow in the EV dark offset. It is produced by CCD sensor and proportional to integration time. Because the OBCBB radiation in the DNB spectral range is sufficiently weak, N_{contam} is assumed to be 0 when the BB dark offset is analyzed using Eq. 1.

As described in Sec. 2, the DNB EV and BB dark offset can be determined from the VROP and OBCBB data. During each monthly VROP, the DNB operates in the so-called test mode for a short time period when the DNB electronics is disconnected from the DNB sensor. The corresponding EV and OBCBB data is effectively recorded under the conditions of zero exposure and closed shutter, consequently only due to the DNB electronics. Processing the DNB test mode data produces electronic bias N_{bias} for both the EV and BB. Once dark offset and electronic bias are determined, relation between the EV and BB dark offset and possible light contamination included in EV dark scenes can be analyzed via Eq. 1. Because the BB dark offset and N_{bias} are per aggregation mode, the EV dark offset and electronic bias are converted to functions of aggregation mode by averaging dark offset and electronic bias of all samples of the same aggregation mode.

It can be seen from Eq. 1 that relationship between the EV and BB HGS dark offsets should be investigated through their dark current and electronic bias components separately. Because the EV HGS dark offset includes unknown airglow which is the light contamination term in Eq. 1, he EV HGS dark current can not be estimated by Eq. 1. Comparison of the EV and BB HGS dark current is difficult. However, dark current is generated in CCD. Only different integration time between the DNB EV and OBCBB view can lead to different dark currents. Considering the MGS EV and BB dark offset consist of certain amount of dark current but are free of light contamination, we used the MGS EV and BB dark current derived by Eq. 1 to investigate if the integration time of the DNB EV and OBCBB view is the same. The MGS EV and BB dark current of aggregation mode 1 are shown in Figure 3. This aggregation mode is selected because it has the most subpixels and therefore the largest dark current among all 32 aggregation modes. The corresponding uncertainties of the calculated dark currents are shown in the figure as well. It can be clearly seen that the time series of two dark currents are close to each other. Although their relative difference (Figure 3b) is 3.67% on average, such difference is much smaller than the uncertainties shown in Figure 2a. Therefore, it can be assumed that there is no observable integration time difference between the DNB EV and OBCBB view. Since dark current is proportional to integration time, we can conclude that the EV and BB HGS dark currents and subsequently their drifts are the same.

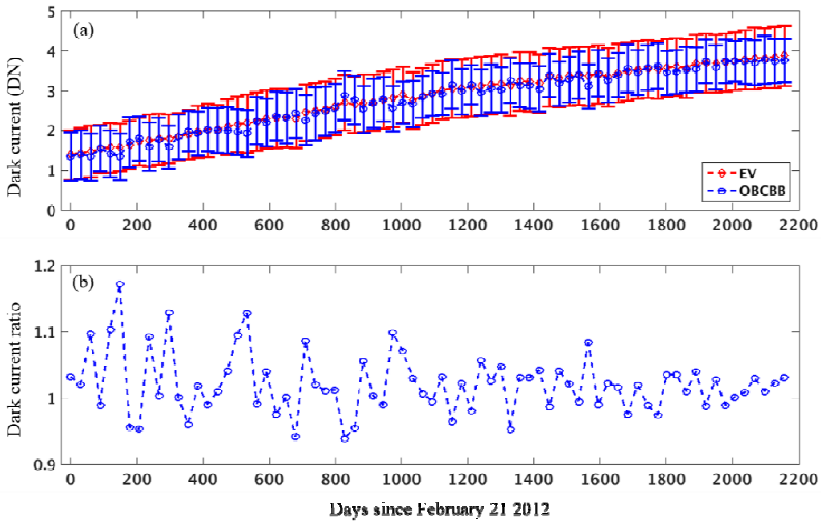

Figure 3. The EV and BB MGS dark current (a) and the corresponding ratio (b). Aggregation mode 1, detector 1 and HAM A.

Equal HGS dark current drift does not guarantee equal HGS dark offset drift. Variation of electronic bias must be considered. In general, the HGS electronic bias drifts of these two views are similar for all detectors of most aggregation modes in the past six years. However, we have found a discrepancy between the EV and BB HGS electronic bias drift for a few detectors in aggregation mode 29 to 32. Figure 4 shows the HGS electronic bias change for aggregation 29 detectors 10 and 11 of two views. It can be seen that the BB bias changes are similar for these two detectors, but the EV bias changes are quite different. As the electronic bias is a part of the dark offset, such different HGS electronic bias change eventually induces different HGS dark offset change, shown in Figure 5. The drifts of the BB HGS dark offset of detectors 10 and 11 are similar. But the drift of the EV HGS dark offset of detector 10 is faster than the counterpart of detector 11. In other word, the EV HGS dark offset drift of detector 10 will be underestimated by its BB HGS dark offset drift, consequently yielding striping in the calibrated DNB nighttime radiance images. In fact, dark offset drift is due to

dark current increase. The BB and EV HGS dark currents of aggregation mode 29 detectors 10 and 11 are shown in Figure 6, calculated by Eq. 1. It should be noted that because the EV HGS dark offset includes unknown airglow (N_{contam}), the EV HGS dark current shown in Figure 6 is the nominal one. It clearly shows that the EV and BB HGS dark currents of these two detectors drift at a similar rate despite of the airglow-induced short-term fluctuations in the EV HGS dark current. Figure 7 shows the correlation coefficient between the BB HGS dark current and the nominal EV HGS dark current for all 32 aggregation modes and 16 detectors. Abnormal correlation appearing in aggregation mode 29 – 32 in Figure 2 disappears in Figure 7. Decrease of the correlation between the BB and the nominal EV HGS dark current from aggregation mode 1 to 32 is due to the increased airglow included in the nominal EV HGS dark current.

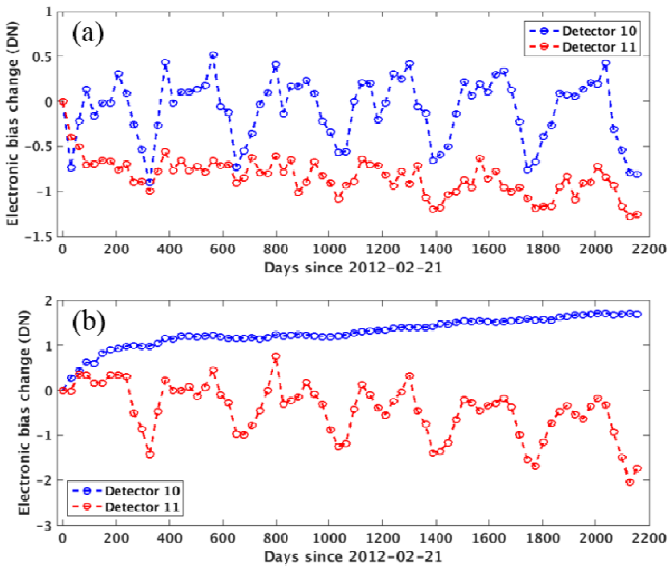

Figure 4. The BB HGS electronic bias change (a) and the EV HGS electronic bias change (b). Aggregation mode 29, detector 10 and 11.

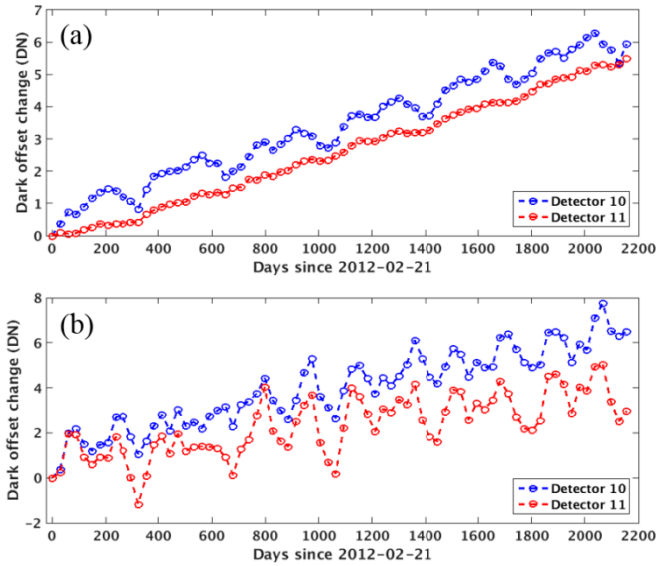

Figure 5. The BB HGS dark offset change (a) and the EV HGS dark offset change (b). Aggregation mode 29, detector 10 and 11, and HAM A.

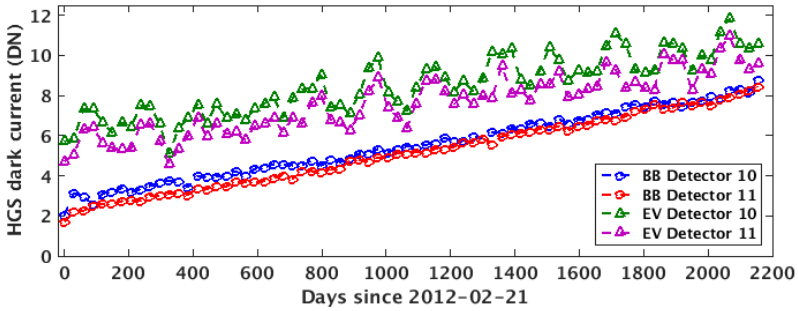

Figure 6. The BB HGS dark current and the nominal EV HGS dark current. Aggregation mode 29, detector 10 and 11, and HAM A.

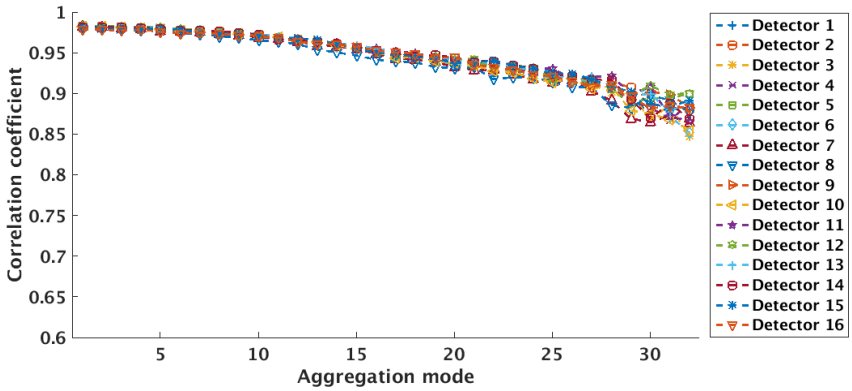

Figure 7. Correlation coefficient between the BB HGS dark current and the nominal EV HGS dark current for all detectors and aggregation modes (HAM A).

4. IMPROVED ALGORITHM FOR DETERMINATION OF DNB HGS DARK OFFSET

Determination of HGS dark offset that is free from light contamination is critical for the DNB low light calibration. It relies on proper selection of dark reference. The OBCBB is sufficiently dark when viewed by the DNB in nighttime around new moon. In addition, it has been shown in Sec. 3 that the dark current component of the BB HGS dark offset can track the EV HGS dark offset change. In this section, we propose an improved algorithm to determine the EV HGS dark offset free from light contamination through combined use of the DNB OBCBB and VROP data.

The basic principle is to use the OBCBB data to estimate and then remove light contamination included in the EV HGS dark offset determined by the original algorithm that uses the VROP data. For every new moon when the DNB test mode data are available, we can calculate the BB HGS dark current by Eq. 1. Meanwhile, we can also calculate the nominal EV HGS dark current by subtracting the EV HGS electronic bias from the EV HGS dark offset determined by the original algorithm. According to Eq. 1, the nominal EV HGS dark current contains dark current and light contamination. However, the BB HGS dark current has been shown to be equal to the EV HGS dark current in Sec. 3. The amount of light contamination can be estimated by the difference between the nominal EV HGS dark current and the BB HGS dark current, expressed by the following equation,

$$\begin{aligned} N_{contam} \quad = \quad & \left[\text{HGS\_dark\_offset\_EV}_{orig} - \text{HGS\_electronic\_bias\_EV}\right] - \\ & \left[\text{HGS\_dark\_offset\_BB} - \text{HGS\_electronic\_bias\_BB}\right], \end{aligned} \tag{2}$$

where $\mathrm{HGS\_dark\_offset\_EV_{orig}}$ is the original EV HGS dark offset determined by the original algorithm. Once the estimated light contamination $\mathrm{N_{contam}}$, is known, the corrected EV HGS dark offset that is free of light contamination can be obtained by simply removing $\mathrm{N_{contam}}$ from the original EV HGS dark offset,

$$\mathrm{HGS\_dark\_offset\_EV_{corr}} = \mathrm{HGS\_dark\_offset\_EV_{orig}} - \mathrm{N_{contam}}. \quad (3)$$

It should be noted that because the BB HGS dark offset and electronic bias are per aggregation, the original EV HGS dark offset and electronic bias used in Eq. 2 are converted to functions of aggregation mode by averaging dark offset and electronic bias of all samples of the same aggregation mode. The calculated $\mathrm{N_{contam}}$ is per aggregation mode. However, the EV HGS dark offset is per sample when used for calibration. $\mathrm{N_{contam}}$ used in Eq. 3 is converted back to functions of sample by assigning the same value for all samples of the same aggregation mode.

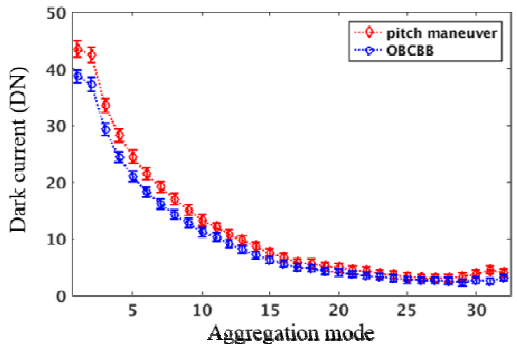

Figure 8. The BB HGS dark current included in the BB HGS dark offset for February 21, 2012 and the nominal EV HGS dark current included in the baseline EV HGS dark offset determined by the DNB pitch maneuver data collected on February 20, 2012. Detector 1 and HAM side A.

In fact, our improved algorithm (Eq. 2) can be used to test if the DNB observation of deep space collected during the spacecraft pitch maneuver on February 20, 2012 is contaminated by star lights. We first calculated the BB HGS dark current in February 21, 2012 through Eq. 2. It is assumed to be the BB HGS dark current in February 20 2012, the day when the spacecraft pitch maneuver was performed, considering negligible dark current change over one day. Meanwhile, we also calculated the nominal EV HGS dark current on February 20, 2012 by subtracting the EV HGS electronic bias on February 21, 2012 from the baseline EV HGS dark offset. Here we also assume negligible change of the EV HGS electronic bias over one day. Both two HGS dark currents are shown in Figure 8. Error bars indicate the corresponding uncertainties of the calculated dark currents. It can be clearly seen that the nominal EV HGS dark current is higher than the BB HGS dark current for all aggregation modes. Since we have shown the same EV and BB HGS dark current, the difference exhibiting in Figure 8 suggests nonzero star light contamination included in the DNB deep space scenes collected during the spacecraft pitch maneuver.

We have reprocessed the historical VROP data to generate the EV HGS dark offsets free from light contamination by our improved algorithm. The results are shown in Figure 9 where the time series of the EV HGS dark offset determined by the original algorithm using the VROP data is also shown. Short-term fluctuations, exhibiting in the original one, have been significantly reduced in the new one. This is attributed to the OBCBB's high stability. Smooth long-term drift of the EV HGS dark offset determined by the improved algorithm could potentially improve the DNB radiometric performance at low radiance level.

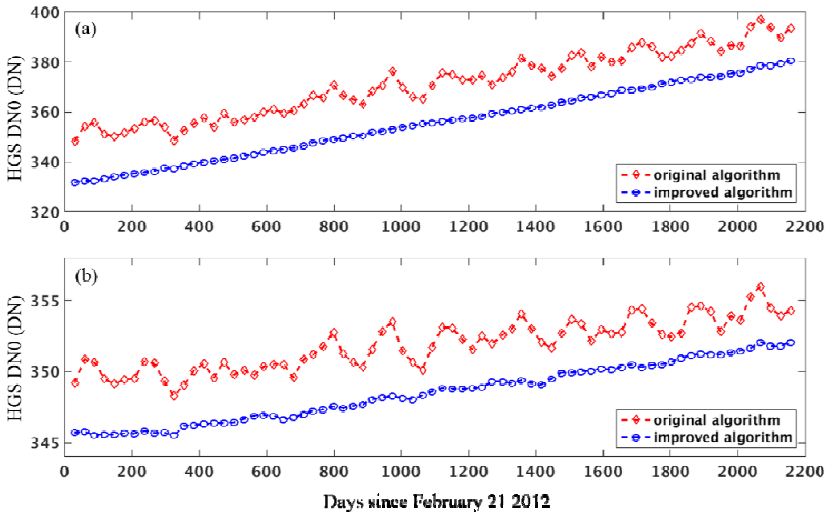

Figure 9. The EV HGS dark offset (DN0) time series determined by the original and improved algorithms. Detector 1, HAM side A, in aggregation mode 1 (a) and 25 (b).

5. CONCLUSIONS

In this paper, we have comprehensively analyzed the relationship between the DNB EV and BB HGS dark offset. Our analysis shows that the BB HGS dark current, which is part of the BB HGS dark offset, must be used with the EV electronic offset to track the on-orbit change of the EV HGS dark offset. We have also shown that the OBCBB in nighttime around new moon is the darkest object available for the DNB EV HGS dark offset determination, better than either deep space or the Pacific Ocean during nighttime of new moon. With these acquired knowledge, an improved algorithm was proposed to determine the DNB HGS dark offset. The improved algorithm does not require the DNB data collected during the spacecraft pitch maneuver. By combined use of the DNB OBCBB data and the DNB VROP data, the generated EV HGS dark offset is free of light contamination and consequently changes smoothly over the whole mission. The improved algorithm could improve both accuracy and stability of the DNB radiometric calibration at low radiance level.

ACKNOWLEDGMENT

This work is funded by the Joint Polar Satellite System program office. The manuscript contents are solely the opinions of the authors and do not constitute a statement of policy, decision, or position on behalf of NOAA or the U.S. government.

REFERENCES

[1] Cao, C., Xiong, J., Blonski, S., Liu, Q., Uprety, S., Shao, X., Bai, Y., and Weng, F., "Suomi NPP VIIRS sensor data record verification, validation, and long-term performance monitoring," J. Geophys. Res. **118**, 11644-11678 (2013).

[2] Liao, L. B., Weiss, S., Mills, S., and Hauss, B., "Suomi NPP VIIRS day-night band on-orbit performance," J. Geophys Res. **118**, 12705-12718 (2013).

[3] Cao, C., Shao, X., and Uprety, S., "Detecting light ourages after severe storms using the S-NPP/VIIRS Day/Night Band radiances," IEEE Geosci. Remote Sens. Lett. 10, 1582-1586 (2013).

[4] Joint Polar Satellite Systems VIIRS Radiometric Calibration Algorithm Theoretical Basis Document, Revision D (2017), https://www.star.nesdis.noaa.gov/jpss/documents/ATBD/D0001-M01-S01-003_JPSS_ATBD_VIIRS-SDR_D.pdf.
[5] Yamashita, A., Dotani, T., Bautz, M., Crew, G., Ezuka, H., Gendreau, K., Kotani, T., Mitsuda, K., Otani, C., Rasmussen, A., Ricker, G., and Tsunemi, H., "Radiation damage to charge coupled devices in the space environment," IEEE Trans. Nucl. Sci. 44, 847 – 853 (1997).
[6] Sun, C., Schwarting, T., Chen, H., Chiang, K., and Xiong, X., "Prediction of S-NPP VIIRS DNB gains and dark offsets," Proc. SPIE 10402, 104021U (2017).
[7] Xiong, X., Butler, J., Chiang, K., Efremove, B., Fulbright, J., Lei, N., McIntire, J., Oudrari H.,, Sun, J., Wang, Z., and Wu, A., "VIIRS on-orbit calibration methodology and performance," J. Geophys. Res. 119, 5065 – 5078 (2014).
[8] Joint Polar Satellite System VIIRS Geolocation Algorithm Theoretical Basis Document, Revision A (2017), https://www.star.nesdis.noaa.gov/jpss/documents/ATBD/D0001-M01-S01-004_JPSS_ATBD_VIIRS-Geolocation.pdf.
[9] Hopkinson, G. R., Goodman, T. M., and Prince, S. R. [A Guide to the Use and Calibration of Detector Array Equipment], SPIE Press (2004).